NPRE 555
Computer Project 3

Roberto E. Fairhurst Agosta
ref3@illinois.edu

December 16, 2020

1 Introduction

For this project, I have implemented kernels in a Multi-physics Object-Oriented Simulation Environment (MOOSE)-based application [1] to solve the Simplified P_3 (SP_3) equations. This report presents the development of those kernels as well as results of one and two-dimensional models. Section 3.a displays the results of the one-dimensional model and compares them against the results obtained with the diffusion solver in Moltres [2]. Section 3.b presents the results of a two-dimensional model of the C5 MOX Benchmark [3].

2 Methodology

This section of the report introduces the followed methodology in the development of this work, comprising the following sections: Section 2.a describes MOOSE framework, Section 2.b outlines SP_3 equations and their translation into kernel form, Section 2.c introduces Moltres and the equations it solves, and Section 2.d presents the C5 MOX Benchmark.

2.a MOOSE

MOOSE is a computational framework that supports engineering analysis applications. In a nuclear reactor, several partial differential equations describe the physical behavior. These equations are typically nonlinear, and they are often coupled to each other. MOOSE targets such systems and solves them in a fully coupled manner.

MOOSE is an open-source Finite Element Method (FEM) framework. The framework itself relies on LibMesh [4] and PetSc [5] for solving nonlinear equations. MOOSE applications define weak forms of the governing equations and modularize the physics expressions into "kernels." Kernels are C++ classes containing methods for computing the residual and Jacobian contributions of individual pieces of the governing equations. MOOSE and LibMesh translate them into residual and Jacobian functions. These functions become inputs into PetSc solution routines.

All the software built on the MOOSE framework shares the same Application Programming Interface (API). The applications, by default, utilize implicit methods [2]. This feature facilitates relatively easy coupling between different phenomena. Additionally, the framework and its applications use Message Passing Interface (MPI) for parallel communication and allow deployment on massively-parallel cluster-computing platforms.

2.b SP_3

Davidson [6] first introduced the one dimensional P_3 equations

$$\frac{d}{dx}\phi_{1,g} + \Sigma_{t,g}\phi_{0,g} = \sum_{g'=1}^{G} \Sigma_{s0,g'\to g}\phi_{0,g'} + \frac{\chi_g}{k_{eff}} \sum_{g'=1}^{G} \nu\Sigma_{f,g'}\phi_{0,g'} + Q_{0,g} \tag{1}$$

$$\frac{1}{3}\frac{d}{dx}\phi_{0,g} + \frac{2}{3}\frac{d}{dx}\phi_{2,g} + \Sigma_{t,g}\phi_{1,g} = \sum_{g'=1}^{G} \Sigma_{s1,g'\to g}\phi_{1,g'} + Q_{1,g} \tag{2}$$

$$\frac{2}{5}\frac{d}{dx}\phi_{1,g} + \frac{3}{5}\frac{d}{dx}\phi_{3,g} + \Sigma_{t,g}\phi_{2,g} = \sum_{g'=1}^{G} \Sigma_{s2,g'\to g}\phi_{2,g'} + Q_{2,g} \tag{3}$$

$$\frac{3}{7}\frac{d}{dx}\phi_{2,g} + \Sigma_{t,g}\phi_{3,g} = \sum_{g'=1}^{G} \Sigma_{s3,g'\to g}\phi_{3,g'} + Q_{3,g} \tag{4}$$

where

$\phi_{n,g} = n^{th}$ moment of the group g neutron flux $[n \cdot cm^{-2} \cdot s^{-1}]$
$\Sigma_{t,g}$ = group g macroscopic total cross-section $[cm^{-1}]$
$\Sigma_{sn,g' \to g} = n^{th}$ moment of the group g' to group g macroscopic scattering cross-section $[cm^{-1}]$
$\nu\Sigma_{f,g}$ = group g macroscopic production cross-section $[cm^{-1}]$
χ_g = group g fission spectrum $[cm^{-1}]$
k_{eff} = multiplication factor $[-]$
$Q_{n,g} = n^{th}$ group g external neutron source $[n \cdot cm^{-3} \cdot s^{-1}]$
G = number of energy groups $[-]$.

Defining the group g "removal" cross-section $\Sigma_{n,g}$, and assuming an isotropic external source and a negligible anisotropic group-to-group scattering [7]

$$\begin{aligned}
&\Sigma_{n,g} = \Sigma_{t,g} - \Sigma_{sn,g' \to g} \\
&Q_{n,g} = 0, \quad n > 0 \\
&\Sigma_{sn,g' \to g} = 0, \quad g' \neq g, \quad n > 0
\end{aligned}$$

the P_3 equations become

$$\frac{d}{dx}\phi_{1,g} + \Sigma_{0,g}\phi_{0,g} = \sum_{g' \neq g}^{G} \Sigma_{s0,g' \to g}\phi_{0,g'} + \frac{\chi_g}{k_{eff}} \sum_{g'=1}^{G} \nu\Sigma_{f,g'}\phi_{0,g'} + Q_{0,g} \tag{5}$$

$$\frac{1}{3}\frac{d}{dx}\phi_{0,g} + \frac{2}{3}\frac{d}{dx}\phi_{2,g} + \Sigma_{1,g}\phi_{1,g} = 0 \tag{6}$$

$$\frac{2}{5}\frac{d}{dx}\phi_{1,g} + \frac{3}{5}\frac{d}{dx}\phi_{3,g} + \Sigma_{2,g}\phi_{2,g} = 0 \tag{7}$$

$$\frac{3}{7}\frac{d}{dx}\phi_{2,g} + \Sigma_{3,g}\phi_{3,g} = 0. \tag{8}$$

Reorganizing equations 6 and 8 allows for obtaining a expression for the odd moments of the flux $\phi_{1,g}$ and $\phi_{3,g}$

$$\phi_{1,g} = -\frac{1}{3\Sigma_{1,g}}\frac{d}{dx}\left[\phi_{0,g} + 2\phi_{2,g}\right] \tag{9}$$

$$\phi_{3,g} = -\frac{3}{7\Sigma_{3,g}}\frac{d}{dx}\phi_{2,g}. \tag{10}$$

With equations 9 and 10, equations 5 and 7 become

$$-D_{0,g}\frac{d^2}{dx^2}\left(\phi_{0,g} + 2\phi_{2,g}\right) + \Sigma_{0,g}\phi_{0,g} = \sum_{g' \neq g}^{G} \Sigma_{s0,g' \to g}\phi_{0,g'} + \frac{\chi_g}{k_{eff}} \sum_{g'=1}^{G} \nu\Sigma_{f,g'}\phi_{0,g'} + Q_{0,g} \tag{11}$$

$$-\frac{2}{5}D_{0,g}\frac{d^2}{dx^2}\left(\phi_{0,g} + 2\phi_{2,g}\right) - D_{2,g}\frac{d^2}{dx^2}\phi_{2,g} + \Sigma_{2,g}\phi_{2,g} = 0 \tag{12}$$

where

$$\begin{aligned}
D_{0,g} &= \frac{1}{3\Sigma_{1,g}} \\
D_{2,g} &= \frac{9}{35\Sigma_{3,g}}.
\end{aligned}$$

Introducing the variables $\Phi_{0,g}$ and $\Phi_{2,g}$ and reorganizing equations 11 and 12 yields

$$-D_{0,g}\frac{d^2}{dx^2}\Phi_{0,g}+\Sigma_{0,g}\Phi_{0,g}-2\Sigma_{0,g}\Phi_{2,g}=S_{0,g} \tag{13}$$

$$-D_{2,g}\frac{d^2}{dx^2}\Phi_{2,g}+\left(\Sigma_{2,g}+\frac{4}{5}\Sigma_{0,g}\right)\Phi_{2,g}-\frac{2}{5}\Sigma_{0,g}\Phi_{0,g}=-\frac{2}{5}S_{0,g} \tag{14}$$

where

$$\Phi_{0,g}=\phi_{0,g}+2\phi_{2,g}$$
$$\Phi_{2,g}=\phi_{2,g}$$
$$S_{0,g}=\sum_{g'\neq g}^{G}\Sigma_{s0,g'\rightarrow g}\left(\Phi_{0,g'}-2\Phi_{2,g'}\right)+\frac{\chi_g}{k_{eff}}\sum_{g'=1}^{G}\nu\Sigma_{f,g'}\left(\Phi_{0,g'}-2\Phi_{2,g'}\right)+Q_{0,g}.$$

The P_N equations yield the exact transport solution as $N\rightarrow\infty$ [7]. In three-dimensional geometries, the number of P_N equations grows like $(N+1)^2$, while in one-dimensional planar geometries, the number of equations is $(N+1)$. The one-dimensional planar P_N equations can be reformulated to yield $(N+1)/2$ coupled equations. This realization lead Gelbard [8] to propose the SP_N approximation. This approximation replaces the second derivatives in the one-dimensional planar P_N equations with three-dimensional Laplacian operators. This approximation yields the following equations for $N=3$ [7]

$$-D_{0,g}\Delta\Phi_{0,g}+\Sigma_{0,g}\Phi_{0,g}-2\Sigma_{0,g}\Phi_{2,g}=S_{0,g} \tag{15}$$

$$-D_{2,g}\Delta\Phi_{2,g}+\left(\Sigma_{2,g}+\frac{4}{5}\Sigma_{0,g}\right)\Phi_{2,g}-\frac{2}{5}\Sigma_{0,g}\Phi_{0,g}=-\frac{2}{5}S_{0,g}. \tag{16}$$

The Marshak vacuum boundary conditions (BCs) complete the system of equations [9]

$$\frac{1}{4}\Phi_{0,g}\pm\frac{1}{2}\hat{n}\cdot J_{0,g}-\frac{3}{16}\Phi_{2,g}=0 \tag{17}$$

$$-\frac{3}{80}\Phi_{0,g}\pm\frac{1}{2}\hat{n}\cdot J_{2,g}+\frac{21}{80}\Phi_{2,g}=0 \tag{18}$$

where

$$J_{n,g}=-D_{n,g}\nabla\Phi_{n,g}.$$

To define MOOSE kernels, the SP_3 equations are translated into weak form multiplying the equations by the test function Ψ and integrating over the domain [10]

$$\langle\Phi,\Psi\rangle=\int_V\Phi\Psi dV \tag{19}$$

$$\langle\Phi,\Psi\rangle_{BC}=\int_S\Phi\Psi dS \tag{20}$$

where

$\Psi=$ test function
$V=$ domain volume
$S=$ boundary surface.

The weak form of equations 15 and 16 becomes

$$\langle -D_{0,g}\Delta\Phi_{0,g},\Psi\rangle + \langle \Sigma_{0,g}\Phi_{0,g},\Psi\rangle + \langle -2\Sigma_{0,g}\Phi_{2,g},\Psi\rangle + \langle -S_{0,g},\Psi\rangle = 0 \tag{21}$$

$$\langle -D_{2,g}\Delta\Phi_{2,g},\Psi\rangle + \left\langle \left(\Sigma_{2,g}+\frac{4}{5}\Sigma_{0,g}\right)\Phi_{2,g},\Psi\right\rangle + \left\langle -\frac{2}{5}\Sigma_{0,g}\Phi_{0,g}D_{2,g},\Psi\right\rangle + \left\langle \frac{2}{5}S_{0,g},\Psi\right\rangle = 0. \tag{22}$$

By means of Green's theorem, equations 21 and 22 become

$$\langle D_{0,g}\nabla\Phi_{0,g},\nabla\Psi\rangle - \langle D_{0,g}\nabla\Phi_{0,g},\Psi\rangle_{BC} + \langle \Sigma_{0,g}\Phi_{0,g},\Psi\rangle + \langle -2\Sigma_{0,g}\Phi_{2,g},\Psi\rangle \tag{23}$$

$$+\left\langle -\sum_{g'\neq g}^{G}\Sigma_{s0,g'\to g}\left(\Phi_{0,g'}-2\Phi_{2,g'}\right),\Psi\right\rangle + \left\langle -\frac{\chi_g}{k_{eff}}\sum_{g'=1}^{G}\nu\Sigma_{f,g'}\left(\Phi_{0,g'}-2\Phi_{2,g'}\right),\Psi\right\rangle + \langle -Q_{0,g},\Psi\rangle = 0 \tag{24}$$

$$\langle D_{2,g}\nabla\Phi_{2,g},\nabla\Psi\rangle - \langle D_{2,g}\nabla\Phi_{2,g},\Psi\rangle_{BC} + \left\langle \left(\Sigma_{2,g}+\frac{4}{5}\Sigma_{0,g}\right)\Phi_{2,g},\Psi\right\rangle + \left\langle -\frac{2}{5}\Sigma_{0,g}\Phi_{0,g},\Psi\right\rangle \tag{25}$$

$$+\left\langle \frac{2}{5}\sum_{g'\neq g}^{G}\Sigma_{s0,g'\to g}\left(\Phi_{0,g'}-2\Phi_{2,g'}\right),\Psi\right\rangle + \left\langle \frac{2}{5}\frac{\chi_g}{k_{eff}}\sum_{g'=1}^{G}\nu\Sigma_{f,g'}\left(\Phi_{0,g'}-2\Phi_{2,g'}\right),\Psi\right\rangle + \left\langle \frac{2}{5}Q_{0,g},\Psi\right\rangle = 0. \tag{26}$$

where the boundary condition terms come from the translation into weak form of equations 17 and 18, giving

$$\langle D_{0,g}\nabla\Phi_{0,g},\Psi\rangle_{BC} = \left\langle \frac{1}{2}\Phi_{0,g}-\frac{3}{4}\Phi_{2,g},\Psi\right\rangle_{BC} \tag{27}$$

$$\langle D_{2,g}\nabla\Phi_{2,g},\Psi\rangle_{BC} = \left\langle -\frac{3}{40}\Phi_{0,g}+\frac{21}{40}\Phi_{2,g},\Psi\right\rangle_{BC}. \tag{28}$$

Table 1 separates equations 24 and 26 into kernels. The BodyForce kernel is part of MOOSE framework. The rest of the kernels were developed as part of this work.

Table 1: SP_3 kernels.

Kernel	Equation 24	Equation 26
P3Diffusion	$\langle D_{0,g}\nabla\Phi_{0,g},\nabla\Psi\rangle$	$\langle D_{2,g}\nabla\Phi_{2,g},\nabla\Psi\rangle$
P3SigmaR	$\langle \Sigma_{0,g}\Phi_{0,g},\Psi\rangle$	$\left\langle \left(\Sigma_{2,g}+\frac{4}{5}\Sigma_{0,g}\right)\Phi_{2,g},\Psi\right\rangle$
P3SigmaCoupled	$\langle -2\Sigma_{0,g}\Phi_{2,g},\Psi\rangle$	$\left\langle -\frac{2}{5}\Sigma_{0,g}\Phi_{0,g},\Psi\right\rangle$
P3InScatter	$\left\langle -\sum_{g'\neq g}^{G}\Sigma_{s0,g'\to g}\left(\Phi_{0,g'}-2\Phi_{2,g'}\right),\Psi\right\rangle$	$\left\langle \frac{2}{5}\sum_{g'\neq g}^{G}\Sigma_{s0,g'\to g}\left(\Phi_{0,g'}-2\Phi_{2,g'}\right),\Psi\right\rangle$
P3FissionEigenKernel	$\left\langle -\frac{\chi_g}{k_{eff}}\sum_{g'=1}^{G}\nu\Sigma_{f,g'}\left(\Phi_{0,g'}-2\Phi_{2,g'}\right),\Psi\right\rangle$	$\left\langle \frac{2}{5}\frac{\chi_g}{k_{eff}}\sum_{g'=1}^{G}\nu\Sigma_{f,g'}\left(\Phi_{0,g'}-2\Phi_{2,g'}\right),\Psi\right\rangle$
BodyForce	$\langle -Q_{0,g},\Psi\rangle$	$\left\langle \frac{2}{5}Q_{0,g},\Psi\right\rangle$
BC Kernel		
Vacuum	$\left\langle \frac{1}{2}\Phi_{0,g}-\frac{3}{4}\Phi_{2,g},\Psi\right\rangle_{BC}$	$\left\langle -\frac{3}{40}\Phi_{0,g}+\frac{21}{40}\Phi_{2,g},\Psi\right\rangle_{BC}$

2.c Moltres

Moltres is a MOOSE-based application initially designed for modeling fluid-fuelled Molten Salt Reactors (MSRs). Moltres inherits all the attributes from MOOSE as its application. Moltres solves arbitrary-group neutron diffusion, delayed neutron precursor concentration, and temperature governing equations. It can solve the equations in a fully-coupled way or solve each system independently, allowing for great flexibility and making it applicable to a wide range of nuclear engineering problems. The development of this work utilized Moltres as a stand-alone neutronics solver, which calculates the scalar flux and the multiplication factor with the following equation

$$\nabla \cdot D_g \nabla \phi_g - \Sigma_g^r \phi_g + \sum_{g' \neq g}^{G} \Sigma_{g' \to g}^s \phi_{g'} + \chi_g^t \sum_{g'=1}^{G} \frac{1}{k_{eff}} \nu \Sigma_{g'}^f \phi_{g'} + Q_g = 0 \tag{29}$$

where

D_g = group g diffusion coefficient $[cm]$
ϕ_g = group g neutron flux $[n \cdot cm^{-2} \cdot s^{-1}]$
Σ_g^r = group g macroscopic removal cross-section $[cm^{-1}]$
$\Sigma_{g' \to g}^s$ = group g' to group g macroscopic scattering cross-section $[cm^{-1}]$
χ_t^p = group g total fission spectrum $[-]$
G = number of discrete energy groups $[-]$
k_{eff} = multiplication factor $[-]$
ν = number of neutrons produced per fission $[-]$
Σ_g^f = group g macroscopic fission cross-section $[cm^{-1}]$
Q_g = group g external neutron source $[n \cdot cm^{-3} \cdot s^{-1}]$.

The vacuum boundary condition [11] states that no neutrons penetrate the boundary in the inward direction — the incoming current density is equal to zero

$$J_g^-(r_s) = \frac{1}{4}\phi_g(r_s) + \frac{D}{2}\hat{n_s} \cdot \nabla \phi_g(r_s) = 0 \tag{30}$$

where

$J_g^-(r)$ = incoming current density $[n \cdot cm^{-2} \cdot s^{-1}]$
r_s = position of the boundary $[cm]$
$\hat{n_s}$ = normal direction to the boundary $[-]$.

2.d C5 MOX Benchmark

The Organisation for Economic Co-operation and Development (OECD)/Nuclear Energy Agency (NEA) developed this benchmark to carry out validation of methods and identify their strengths, limitations, and accuracy, and to suggest needs for method development. The definition of the original benchmark can be found in [12]. Capilla et al [3] developed a simplified version of the benchmark using a two-energy group structure, leading to the C5G2 MOX Benchmark.

Figures 1 and 2 display the configuration of the benchmark exercise. Tables 2 and 3 present the cross-sections necessary to carry out the exercise.

3 Results

This sections presents the results for the one-dimensional (1-D) and two-dimensional (2-D) models.

3.a 1-D test case

Figure 3 displays the neutron flux for one and three energy groups for a fixed source case. Figure 4 shows the neutron flux for one and three energy groups for an eigenvalue problem. Table 4 compares the eigenvalue obtained with the SP3 and the diffusion solvers by calculating their difference with the formula

$$\Delta_\rho = |\rho_{SP_3} - \rho_{Ref}| = \left| \frac{k_{SP_3} - 1}{k_{SP_3}} - \frac{k_{Ref} - 1}{k_{Ref}} \right| = \left| \frac{k_{SP_3} - k_{Ref}}{k_{SP_3} k_{Ref}} \right| \tag{31}$$

vacuum

	R	R	R	R	R	R
	R	UO_2	MOX	MOX	UO_2	R
	R	MOX	UO_2	UO_2	MOX	R
vacuum	R	MOX	UO_2	UO_2	MOX	R vacuum
	R	UO_2	MOX	MOX	UO_2	R
	R	R	R	R	R	R

vacuum

Figure 1: 2-D C5 MOX benchmark configuration. Image reproduced from [3]. R represents the reflectors.

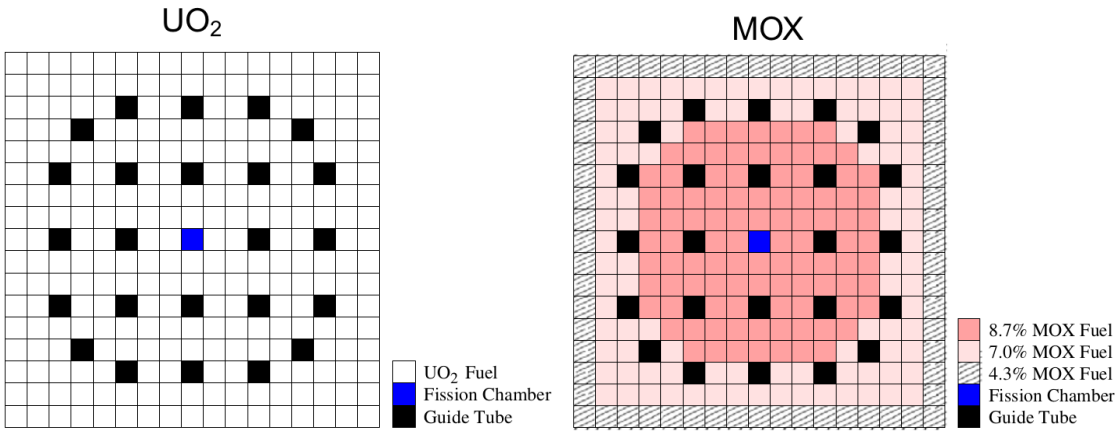

(a) UO_2 assembly.

(b) MOX assembly.

Figure 2: Structure of the UO_2 and MOX assemblies. Images reproduced from [3].

Table 2: Two-group cross-sections $[cm^{-1}]$ for the heterogeneous problem.

Pin cell type	Group	Σ_t	$\nu\Sigma_f$	$\Sigma_{s0,1\to g}$	$\Sigma_{s0,2\to g}$
4.3% MOX	1	0.550	0.0075	0.520	0.000
	2	1.100	0.3000	0.015	0.900
7.0% MOX	1	0.550	0.0075	0.520	0.000
	2	1.010	0.3750	0.015	0.760
8.7% MOX	1	0.550	0.0075	0.520	0.000
	2	1.060	0.4500	0.015	0.760
UO_2	1	0.570	0.0050	0.540	0.000
	2	1.100	0.1250	0.020	1.000
Guide tube	1	0.586	0.0000	0.560	0.000
	2	1.220	0.0000	0.025	1.200
Reflector	1	0.611	0.0000	0.560	0.000
	2	2.340	0.0000	0.050	2.300
Fission chamber	1	0.586	10^{-7}	0.560	0.000
	2	1.220	3×10^{-6}	0.025	1.200

Table 3: Two-group cross-sections $[cm^{-1}]$ for the heterogeneous problem.

Pin cell type	Group	Σ_t	$\nu\Sigma_f$	$\Sigma_{s0,1\to g}$	$\Sigma_{s0,2\to g}$
MOX	1	0.560749	0.006952	0.530682	0.000000
	2	1.064663	0.339038	0.016025	0.836469
UO_2	1	0.573135	0.004589	0.543383	0.000000
	2	1.110761	0.113071	0.020463	1.018406

where

$$k_{SP_3} = \text{eigenvalue obtained with SP3 solver}[-]$$
$$k_{Ref} = \text{eigenvalue obtained with diffusion solver}[-].$$

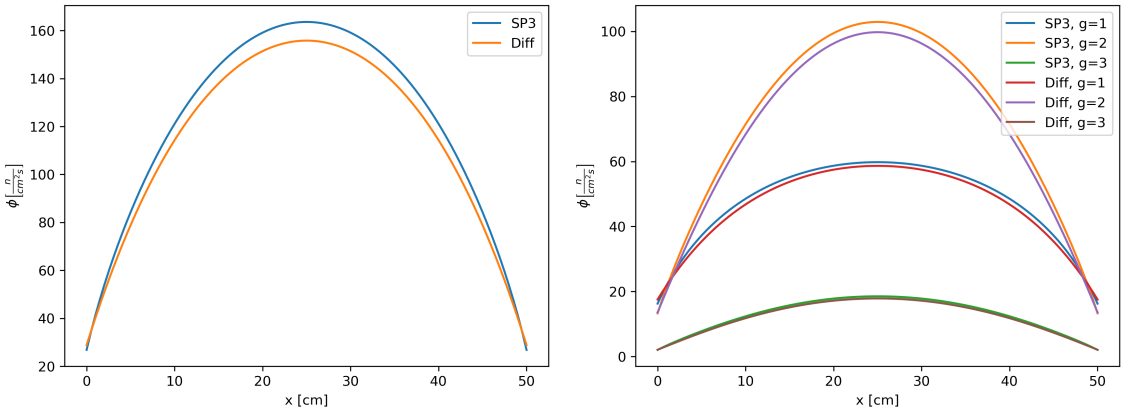

(a) 1 group. (b) 3 groups.

Figure 3: Comparison of the scalar flux obtained with the SP3 and diffusion solvers for the fixed source case.

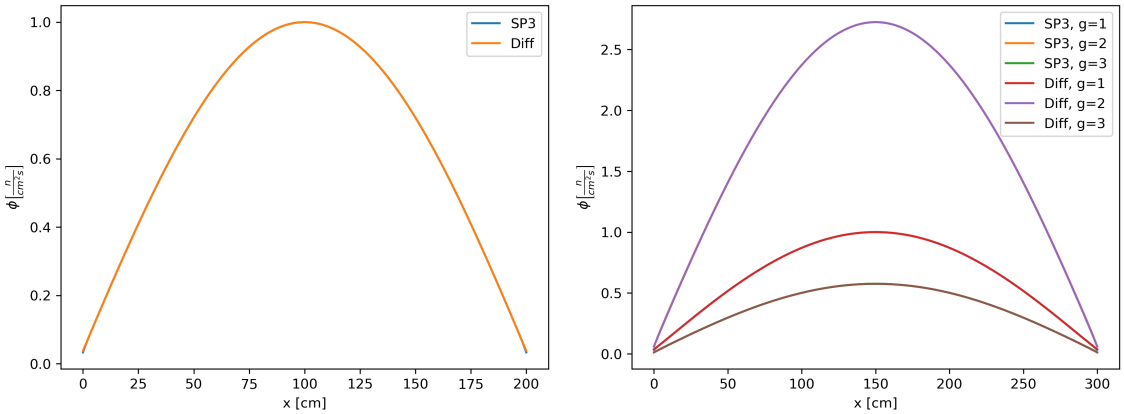

(a) 1 group. (b) 3 groups.

Figure 4: Comparison of the scalar flux obtained with the SP3 and diffusion solvers for the eigenvalues problem.

Table 4: Comparison between the eigenvalue obtained with the SP3 and diffusion solvers.

	Moltres	SP3	
Number of groups	k_{Ref}	k_{SP_3}	Δ_ρ [pcm]
1	1.05278	1.06004	650
3	1.02878	1.03005	120

3.b 2-D test case

Figure 5 displays the scalar flux of the C5G2 MOX Benchmark. Table 5 compares the eigenvalue obtained with the SP3 solver (k_{P_3}) and the results in [3] (k_{Ref}) by using equation 31.

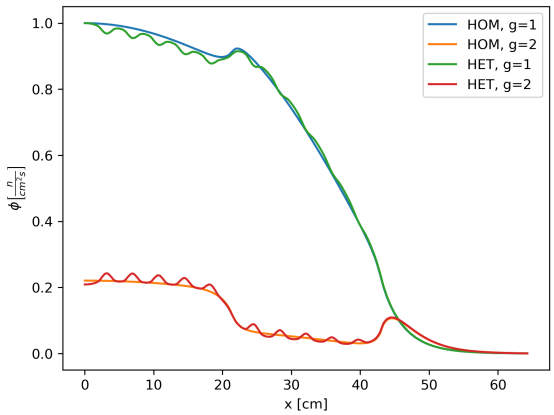

Figure 5: Scalar flux on line between points (0, 10.71) and (64.26, 10.71). HOM: homogeneous case, HET: heterogeneous case.

Table 5: Comparison between the eigenvalue obtained with the SP3 solver and the results in [3].

	C5G2 Benchmark	SP3	
Case	k_{Ref}	k_{SP_3}	Δ_ρ [pcm]
Heterogeneous	0.96969	0.97106	145
Homogeneous	0.96983	0.97061	83

4 Conclusions

Section 3.b results seem to indicate that the implementation of the SP_3 equations in a MOOSE-based application is correct. On the other hand, the results from Section 3.a show that the solution of the SP_3 equations yield very similar scalar fluxes to the diffusion equations. While the diffusion solver calculates the flux with only one equation for each group, the SP_3 equations use two. These characteristics would indicate that the diffusion solver is preferable over the SP_3 solver, yielding similar results by using less degrees of freedom to solve a problem.

References

[1] D. Gaston, C. Newman, G. Hansen, and D. Lebrun-Grandié, "MOOSE: A parallel computational framework for coupled systems of nonlinear equations," *Nuclear Engineering and Design*, vol. 239, pp. 1768–1778, Oct. 2009.

[2] A. Lindsay, G. Ridley, A. Rykhlevskii, and K. Huff, "Introduction to Moltres: An application for simulation of Molten Salt Reactors," *Annals of Nuclear Energy*, vol. 114, pp. 530–540, Apr. 2018.

[3] M. Capilla, D. Ginestar, and G. Verdú, "Applications of the multidimensional equations to complex fuel assembly problems," *Annals of Nuclear Energy*, vol. 36, pp. 1624–1634, Oct. 2009.

[4] B. S. Kirk, J. W. Peterson, R. H. Stogner, and G. F. Carey, "libMesh : a C++ library for parallel adaptive mesh refinement/coarsening simulations," *Engineering with Computers*, vol. 22, pp. 237–254, Dec. 2006.

[5] Balay, Brune, Buschelman, Gropp, Karpeyev, Knepley, C. McInnes, Rupp, Smith, and Zhang, "PETSc Users Manual," Tech. Rep. ANL-95/11 Rev 3.14, Argonne National Laboratory (ANL), Lemont, IL, Apr. 2016.

[6] B. Davidson, *Neutron Transport Theory*. London: Oxford University Press, 1957.

[7] P. Brantley and E. Larsen, "The Simplified P3 Approximation," *Nuclear Science and Engineering*, 2000.

[8] E. Gelbard, "Application of spherical harmonics methods to reactor problems," Technical Report WAPD-BT-20, Bettis Atomic Power Laboratory, 1960.

[9] C. Beckert and U. Grundmann, "Development and verification of a nodal approach for solving the multigroup P3 equations," *Annals of Nuclear Energy*, 2007.

[10] INL, "Moose Workshop Slides," Dec. 2020. https://mooseframework.inl.gov/workshop.

[11] J. J. Duderstadt and L. J. Hamilton, *Nuclear Reactor Analysis*. New York: Wiley, 1 edition ed., Jan. 1976.

[12] OECD/NEA, "Benchmark on Deterministic Transport Calculations Without Spatial Homogenisation: A 2-D/3-D MOX Fuel Assembly Benchmark," Technical Report NEA/NSC/DOC(2003)16, OECD, 2003.